

CHANDRA HETG SPECTRA OF SN 1987A AT 20 YEARS

D. DEWEY,¹ S. A. ZHEKOV,^{2,3} R. MCCRAY,² AND C. R. CANIZARES¹

Received 2007 December 19; accepted 2008 February 15; published 2008 March 7

ABSTRACT

We have undertaken deep, high-resolution observations of SN 1987A at ≈ 20 years after its explosion with the *Chandra* HETG and LETG spectrometers. Here we present the HETG X-ray spectra of SN 1987A having unprecedented spectral resolution and signal-to-noise ratios in the 6–20 Å bandpass, which includes the H-like and He-like lines of Si, Mg, and Ne, as well as O VIII lines and bright Fe XVII lines. In joint analysis with LETG data, we find that there has been a significant decrease from 2004 to 2007 in the average temperature of the highest temperature component of the shocked-plasma emission. Model fitting of the profiles of individual HETG lines yields bulk kinematic velocities of the higher-Z ions, Mg and Si, that are significantly lower than those inferred from the LETG 2004 observations.

Subject headings: ISM: individual (SN 1987A) — radiation mechanisms: thermal — supernova remnants — techniques: spectroscopic — X-rays: ISM

1. INTRODUCTION

Twenty years after outburst, SN 1987A is now well into its supernova remnant phase, such that its observed luminosity is dominated by the impact of the supernova debris with its circumstellar medium (McCray 2007),⁴ and the X-ray luminosity has brightened by a factor of ~ 25 since first observed by *Chandra* in 1999 (Aschenbach 2007) and is currently brightening at a rate of $\sim 40\%$ per year (Park et al. 2007). The X-ray image seen by *Chandra* is an expanding elliptical ring; its brightness distribution is correlated with the rapidly brightening optical hot spots on the inner circumstellar ring seen with the *Hubble Space Telescope*. Assuming that the X-ray emission is a circle inclined at 45° (north side toward Earth), its inferred radial velocity is currently 1412 ± 354 km s⁻¹ (Park et al. 2007).

Michael et al. (2002) reported the first observation of the X-ray spectrum taken with the High Energy Transmission Grating (HETG) on *Chandra* in 1999 October. That observation, of 116 ks duration, showed that the X-rays had an emission-line spectrum characteristic of shocked gas. But that spectrum had insufficient counting statistics (e.g., only 19 counts in O VIII Ly α) to provide reliable line profiles or accurate line ratios. As the X-ray luminosity of SN 1987A has continued to increase, it has become possible to measure emission-line ratios and profiles with sufficient accuracy to permit quantitative interpretation of the shock interaction responsible for the X-ray emission. Dispersed X-ray spectra of SN 1987A have been obtained with the Reflection Grating Spectrometer on *XMM-Newton* in 2003 May (Haberl et al. 2006) and again in 2007 January (Heng et al. 2008), and with the Low Energy Transmission Grating (LETG) on *Chandra* (289 ks duration) in 2004 August–September (Zhekov et al. 2005, 2006; hereafter Z05, Z06).

With angular resolution FWHM $\sim 0.7''$, *Chandra* can resolve the circumstellar ring ($1.2'' \times 1.6''$) of SN 1987A. This angular resolution is vital for interpreting the line widths seen in the dispersed X-ray spectra, which are a convolution of the spatial structure of the X-ray image and the kinematics of the X-ray-

emitting gas. As Z05 have described, one can separate these contributions by comparing the $m = +1$ and $m = -1$ orders of the dispersed spectrum: with the dispersion axis along the north-south direction, the images of the ring in spectral orders dispersed to the north will be “compressed,” and those to the south will be “stretched” (Z05).

We have obtained new *Chandra* spectra of SN 1987A, in 2007 March with the HETG (HETG’07) and in 2007 September with the LETG (LETG’07). In this Letter we focus on the HETG results, which have substantially greater counting statistics and better spectral resolution than the LETG’04 spectra (Z05), and which lead to a significant clarification of Z05’s inferred relationship between bulk motion and ion species. Moreover, we see significant evolution of the thermal structure of the interaction since the 2004 observations. Preliminary analysis of the LETG’07 data confirms that this evolution is not an effect of the spectrometer being used. In a subsequent paper, we will provide a more detailed analysis and interpretation of the combined HETG and LETG observations.

2. OBSERVATIONS AND DATA REDUCTION

The HETG’07 observations were carried out as part of the GTO program in the spring of 2007 near a roll angle of 270° , imaging the “stretched” orders on the ACIS-S1 BI chip (which has the best low-energy sensitivity). The data consist of 14 observations with roll angles from 270° to 238° during SN days 7321–7358, for a total live time of 354.9 ks. We used the standard CIAO tools and HETG extraction procedures to process the data sets. The `tgdetect` routine located the zeroth order near the “dark center” of each event image to better than $0.1''$. The nominally extracted first-order spectra contain the following numbers of counts: 15.2 k (MEG–1), 14.0 k (MEG+1), 5.8 k (HEG–1), and 4.7 k (HEG+1). In Figure 1 we display all four first-order counts spectra in the high-S/N range, 5.5–19.5 Å. The higher resolution and lower effective area of HEG compared to MEG spectra are evident, e.g., at the Ne triplet ~ 13.5 Å; we also display close-ups of the beautifully resolved He-like triplets for Si and Mg in Figure 2.

3. SHOCK EMISSION MEASURE DISTRIBUTION

Following the analysis procedures of Z06, we performed global fits to the data with two models: (1) a simple two-shock

¹ Kavli Institute, Massachusetts Institute of Technology, Cambridge, MA 02139; dd@space.mit.edu, crc@mit.edu.

² JILA, University of Colorado, Boulder, CO 80309-0440; zhekovs@colorado.edu, dick@jila.colorado.edu.

³ On leave from Space Research Institute, Sofia, Bulgaria.

⁴ See also the “Program” link at <http://astrophysics.gsfc.nasa.gov/conferences/supernova1987a/>.

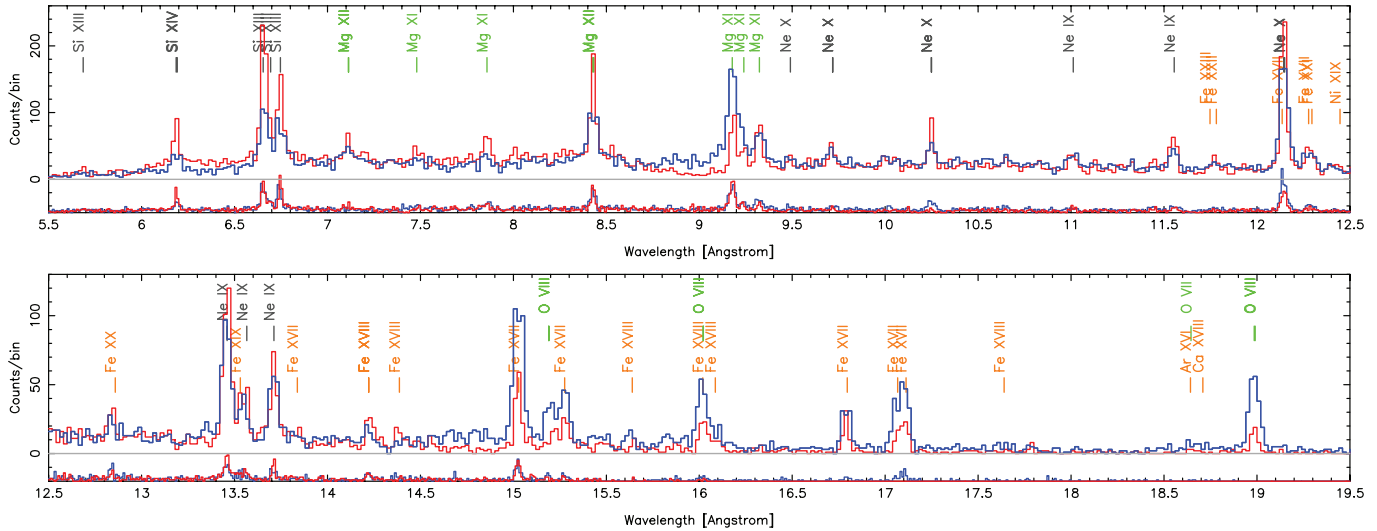


FIG. 1.—HETG SN 1987A spectra. Observed counts spectra from all of the observations, totaling 360 ks, are shown; the MEG minus (blue) and plus (red) order spectra are plotted along with offset HEG spectra (same color coding). The MEG (HEG) bin size is 0.020 (0.010) Å, equivalent to $\approx 1''$ in spatial extent. The wavelengths of expected bright lines are indicated as well.

model and (2) a distribution of shock emission measures model, $EM(T)$. In the latter model, the basic vectors characterizing the spectral distribution are plane-parallel shocks characterized by their mean postshock temperature and a related ionization timescale.

We simultaneously fit the six background-subtracted ± 1 st-order spectra from the LETG'04, HETG'07 (MEG), and LETG'07 data sets, rebinning all spectra to have a minimum of 30 counts per bin. We assumed common values among the data sets for N_{H} , the interstellar absorption column density, as well as the chemical composition of the hot, shocked plasma. Specifically, we fixed the abundances⁵ of H, He, C, Ar, Ca, and Ni to the values given in Z06, and we allowed the abundances of N, O, Ne, Mg, Si, S, and Fe to vary in our fits.

In principle some evolution of the chemical composition might take place as a result of evaporation of dust grains in the shocked gas. However, as Dwek & Arendt (2007) have shown, the dust grains in SN 1987A appear to have such low abundance that they cannot contribute substantially to the gas-phase abundance of heavy elements. Likewise we are assuming

⁵ We specify abundances relative to the AG89 values. It is possible to use another reference set; however, in that case the “fixed” values must be converted to the new system to maintain the same elemental number ratios.

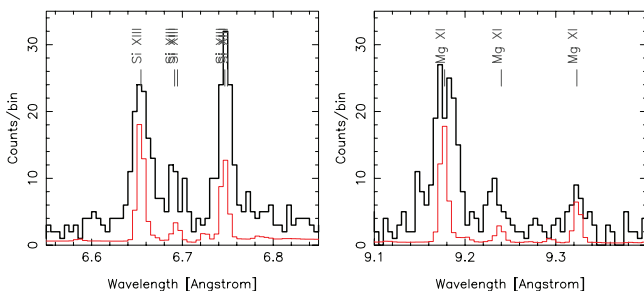


FIG. 2.—Si and Mg triplets resolved. The Si (left) and Mg (right) triplets are plotted as observed in the plus (“compressed”) order of the HEG. The data are shown by the solid black histogram and an arbitrarily scaled point-source version of the two-shock model (no spatial-velocity effects) is shown in red to suggest the relative similarity of the data and model G -ratios $[(f + i)/r]$.

uniformity of composition throughout the ring. These assumptions of stationary and uniform abundances in time and space are taken as a starting point for these analyses.

For the two-shock model joint fits, the derived values and 90% confidence limits (in parentheses) for the absorption column density [$N_{\text{H}} = 1.30 (1.18\text{--}1.46) \times 10^{21}$] and elemental abundances [$N = 0.56 (0.50\text{--}0.65)$, $O = 0.081 (0.074\text{--}0.092)$, $Ne = 0.29 (0.27\text{--}0.31)$, $Mg = 0.28 (0.26\text{--}0.29)$, $Si = 0.33 (0.32\text{--}0.35)$, $S = 0.30 (0.24\text{--}0.36)$, and $Fe = 0.195 (0.189\text{--}0.206)$] are all within or very near the 90% limits presented in Z06. The values of kT_{low} (keV) are very similar for all three data sets: 0.53 (0.50–0.55), 0.56 (0.53–0.59), and 0.54 (0.53–0.56) for the LETG'04, HETG'07, and LETG'07 data, respectively. In contrast, the kT_{high} (keV) values indicate a general evolution toward lower values across these same data sets: 2.7 (2.5–3.0), 2.4 (1.9–2.7), and 1.9 (1.8–2.0).⁶ This result confirms a similar trend seen in the kT (hard) values derived from ACIS monitoring of SN 1987A (Park et al. 2006, 2007).

The decrease in kT_{high} is echoed by an evolution of the shock emission measure distributions, $EM(T)$, that we derive from global fits to the three data sets (Fig. 3). First, note that the fits to the 2007 LETG and MEG data are very similar. The value of $EM(T)$ derived from LETG'07 data is slightly greater than that derived from the 2007 MEG because the source brightened by a factor ≈ 1.17 between 2007 March and April and 2007 September. We see more substantial evolution in $EM(T)$ from 2004 to 2007. Like the 2004 $EM(T)$, the 2007 $EM(T)$ is bimodal, having a low-temperature peak at 0.55 keV and a high-temperature peak at ~ 2 keV. During the interval 2004 September to 2007 March–April, the shape of the low-temperature peak did not change, but the total emission brightened by a factor ~ 2.47 , corresponding to a doubling timescale of approximately 2 years. At higher temperatures the shape of the $EM(T)$ appears to have evolved substantially in addition to the increased amplitude. We see substantial “filling in” of emission measure in the intermediate T range, 1.0–2.5 keV,

⁶ For completeness the joint fit has $\chi^2 = 1819$ for 2248 degrees of freedom, and the $\tau = n_e t$ values (in $10^{11} \text{ s cm}^{-3}$) show an increasing (older, denser) trend, as expected: $\tau_{\text{low}} = 3.2, 3.6, \text{ and } 4.8$; $\tau_{\text{high}} = 1.6, 2.2, \text{ and } 2.7$.

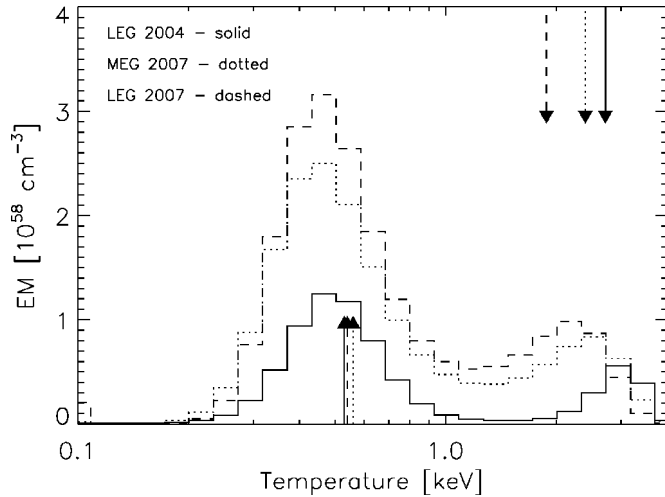


FIG. 3.—Emission measure distribution versus shock temperature. $EM(T)$ as derived with 25 points logarithmically spaced in the 0.1–4 keV postshock temperature range. A disproportionate growth of $EM(T)$ is seen in the mid- T range, ~ 1.4 keV. For reference, the arrows indicate the postshock temperatures of the simple two-shock model fits given in the text; low (high) temperature components are plotted from the lower (upper) x -axis.

and a decrease in the highest temperature bin (>3 keV). Further analysis will be needed to quantify the significance of these apparent changes.

4. LINE PROFILES: EXPANDING RING MODEL

We fit the observed line profiles with a simple model incorporating the basic spatial-kinematic properties of SN 1987A’s geometry, enabling us to infer an average expansion velocity, v_{ring} , for each emission line. The geometric model is a torus with specified inner (1.55”) and outer (1.7”) diameters with its axis oriented in space (42.8° south and 10° east from the line of sight.) The torus has a nonuniform azimuthal intensity distribution determined from the observed zeroth-order imaging data. Emission at each location on the ring is Doppler shifted by the combination of the component of radial expansion at that point along the line of sight, the overall systemic velocity, and an additional Gaussian Doppler broadening term, Δv_{los} , along the line of sight.

We implemented the above as a custom model⁷ in ISIS (Houck 2002). We use a Monte Carlo scheme to evaluate the line profile for the particular model parameters, also taking into account the properties of the specific data set (the grating, order, and observation roll angle.) We sum one (or two in the case of blended lines) of these “ring model” line shapes with the nominal two-shock model in which the abundance of the element being fit is set to zero. We tie the two-shock norms together in the appropriate ratio and allow them to vary in the line fitting. In this way, we have an accurate continuum shape and also make some allowance for contaminating lines, e.g., Fe lines in the Ne triplet region.

We fit the data from the first 319 ks (excluding the last observation taken at a roll angle 25° from the average) with this model in a limited wavelength region around each line. We used all four HEG/MEG ± 1 st-order spectra except in the long-wavelength range ($>16 \text{ \AA}$), where we excluded one or both of the HEG spectra from the fits because of a lack of

⁷ The convenient creation and usage of 3D geometric models in astrophysical data analysis is one component of the Hydra project at MIT; see, e.g., <http://space.mit.edu/hydra/v3d.html>.

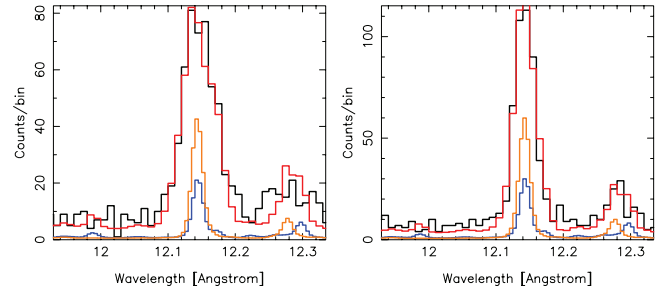


FIG. 4.—Example of the spatial-spectral model fit. The MEG minus (left) and plus (right) order data (black) for the Ne x line are shown with the best-fit model overplotted (red). For reference, the low- and high- T components of the two-shock model are shown at point-source resolution (orange and blue, respectively).

counts. Figure 4 illustrates the fit to the Ne x line in the MEG ± 1 st-order spectra. We tabulate the results for the bright lines in the spectrum in Table 1 and display their ring expansion velocities in Figure 5. The best-fit values for the additional Doppler broadening parameter, Δv_{los} (not tabulated), are in the 300–700 km s^{-1} FWHM range.

The bulk velocities measured with the HETG’07 data (the diamond symbols in Fig. 5) are significantly lower, by a factor of 2 at Si and Mg, than those inferred from the “stratified” model that was employed to fit the LETG’04 FWHM data (dashed line). The new HETG data are, however, in good agreement with the constant velocity model of Z05 (dotted line). Note that there is the hint of a much reduced “stratified” trend: expansion velocities tending to increase toward shorter wavelengths.

TABLE 1
FIT PARAMETERS FOR THE NONUNIFORM RING MODEL

| Ion | λ_r^a | $\lambda_{\text{fit}}^b (1 \sigma)$ | $v_{\text{ring}}^c \pm 1 \sigma$ | Flux ^d |
|------------------------------|---------------|-------------------------------------|----------------------------------|-------------------|
| Si xiv Ly α | 6.183 | 6.181(1) | 456 (322–641) | $4.6 \pm 10\%$ |
| Si xiii r ^e | 6.648 | 6.650(1) | 450 (370–574) | $14.5 \pm 5\%$ |
| and Si xiii i | 6.687 | 6.691(5) | 450 (370–574) | $3.4 \pm 16\%$ |
| Si xiii f | 6.740 | 6.738(1) | 203 (0–360) | $6.3 \pm 9\%$ |
| Mg xii Ly α | 8.422 | 8.421(1) | 380 (302–471) | $11.0 \pm 6\%$ |
| Mg xi r ^e | 9.169 | 9.170(1) | 303 (230–375) | $22.3 \pm 5\%$ |
| and Mg xi i | 9.230 | 9.228(3) | 303 (230–375) | $5.3 \pm 15\%$ |
| Mg xi f | 9.314 | 9.315(2) | 357 (230–516) | $7.0 \pm 12\%$ |
| Ne x Ly β | 10.239 | 10.241(2) | 396 (267–533) | $10.8 \pm 10\%$ |
| Ne ix (3–1) | 11.544 | 11.545(2) | 32 (0–194) | $11.0 \pm 12\%$ |
| Ne x Ly α | 12.135 | 12.134(1) | 375 (309–439) | $72.0 \pm 4\%$ |
| Ne ix r ^e | 13.447 | 13.448(1) | 253 (146–323) | $62.0 \pm 6\%$ |
| and Ne ix i | 13.552 | 13.552(3) | 253 (146–323) | $16.0 \pm 16\%$ |
| Ne ix f | 13.699 | 13.698(1) | 189 (121–282) | $36.7 \pm 9\%$ |
| Fe xvii | 15.014 | 15.014(1) | 361 (295–411) | $75.0 \pm 6\%$ |
| O viii Ly β | 16.006 | 16.006(3) | 539 (434–648) | $42.6 \pm 11\%$ |
| Fe xvii | 16.780 | 16.775(3) | 260 (170–344) | $33.5 \pm 13\%$ |
| Fe xvii ^e | 17.051 | 17.051(4) | 123 (60–304) | $27.4 \pm 17\%$ |
| and Fe xvii | 17.096 | 17.094(3) | 123 (60–304) | $41.7 \pm 13\%$ |
| O viii Ly α | 18.970 | 18.970(3) | 172 (70–272) | $103.0 \pm 10\%$ |
| O vii r | 21.602 | 21.60(1) | 259 (0–431) | $28.0 \pm 40\%$ |
| O vii f | 22.098 | 22.01(1) | 208 (0–350) | $33.0 \pm 40\%$ |
| N vii Ly α | 24.782 | 24.77(1) | 189 (45–333) | $75.0 \pm 22\%$ |

^a Theoretical wavelengths in \AA , from Huenemoerder et al. (2006).

^b Measured wavelengths in \AA with last-digit error in parentheses. Doppler and systematic (286.5 km s^{-1}) velocities are then included in the model.

^c This is the model radial velocity, in km s^{-1} , in the equatorial plane at the average ring radius and its $\pm 1 \sigma$ range.

^d Observed flux in $10^{-6} \text{ photons cm}^{-2} \text{ s}^{-1}$.

^e Two lines were jointly fit for this closely spaced pair.

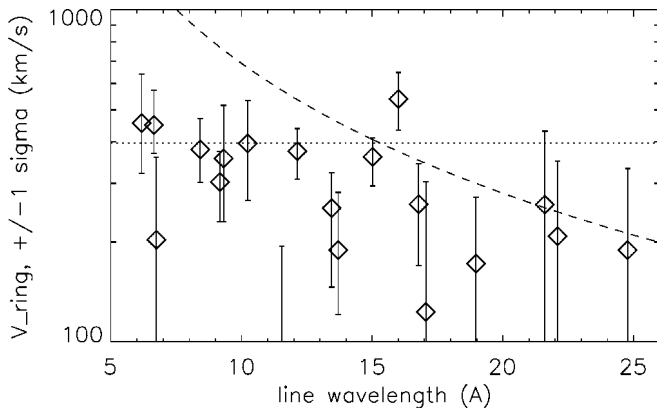


FIG. 5.—“Ring” velocities vs. wavelength. The HETG-measured radial velocities and their 1σ ranges are plotted against the line wavelength. For comparison the “stratified” (dashed line) and “constant” (dotted line) radial velocities from Z05 are overplotted. The stratified model is clearly excluded by the new HETG data.

5. DISCUSSION

The most striking result that we find from the HETG data is the relatively low bulk radial velocity of the shocked gas in the ring. In a simple model consisting of a plane-parallel strong shock entering a stationary gas, the bulk velocity of the shocked thermal plasma should be given by $v_{\text{ps}} = \frac{3}{4}v_{\text{sh}}$, and the postshock mean plasma temperature should be given by $kT = 1.4(v_{\text{sh}}/1000 \text{ km s}^{-1})^2 \text{ keV}$ (for mean molecular weight $\mu = 0.72$ based on our abundances, see also Z06). Then, setting $v_{\text{ps}} = v_{\text{ring}}$, we would expect postshock temperatures in the range $kT \sim 0.1\text{--}0.6 \text{ keV}$ for the observed range $v_{\text{ring}} \sim 200\text{--}500 \text{ km s}^{-1}$ (Fig. 5). This temperature range is much lower than the range $0.3\text{--}3 \text{ keV}$ inferred from the spectral modeling of the emitting gas. Clearly, such a simple shock model is inadequate to describe the actual system.

The range of broadening Δv_{los} used in the fits to the line profile, $300\text{--}700 \text{ km s}^{-1}$ FWHM, generally exceeds the expected thermal line-of-sight contribution, given by $\Delta v_{\text{therm}} = 163[E_{\text{keV}}/(A/20)]^{1/2} \text{ km s}^{-1}$ FWHM, where $E_{\text{keV}} = kT_i$ is the ion temperature in keV and A is the atomic weight of the ion. For $E_{\text{keV}} = 0.4\text{--}3$ the range of thermal Doppler widths (FWHM) is $115\text{--}315$ (O), $87\text{--}237$ (Si), and $61\text{--}170$ (Fe).

The fact that the X-ray image is correlated with the optical hot spots leads us to a picture in which the blast wave ahead of the supernova debris is overtaking dense clumps of circumstellar gas associated with the hot spots. Since these hot spots are unresolved, we can only guess at their geometry and density distribution. But it would be reasonable to expect that the X-ray-emitting gas spans a range of densities and has complex morphology.

If a blast wave runs into a clump of high density at *normal incidence*, the transmitted shock might be too slow to emit X-rays but the shock encountering the clump would be reflected. The reflected shock would leave behind twice-shocked gas having nearly stationary bulk velocity but further elevated temperature. As more and more of the X-ray emission comes from gas behind such reflected shocks, we would expect that the fraction of the X-ray emission measure at higher temperatures would increase, while the average bulk velocity would decrease. And that is what we see.

In addition, much of the X-ray emission probably comes from shocks resulting from the blast wave encountering dense clumps at *oblique incidence*, in which case the shocked gas would have significant velocity components parallel to the shock surface. We suspect that the complex hydrodynamics resulting from both transmitted and reflected shocks encountering the circumstellar ring at normal and oblique incidence is responsible for the Doppler broadening seen in the line profiles.

As Table 1 shows, the radial expansion velocity of the ring inferred from the X-ray line profiles ranges from ~ 200 to 450 km s^{-1} , much less than the value $1412 \pm 354 \text{ km s}^{-1}$ inferred from the expansion of the X-ray image (Park et al. 2007). The expansion of the X-ray image tells us the location of the centroid of the X-ray-emitting ring, which is determined by the average radius of the relatively dense ($n > 10^4 \text{ cm}^{-3}$) shocked gas. We believe that these dense clumps or fingers are being overtaken by a blast wave that is propagating at radial velocities $v > 2000 \text{ km s}^{-1}$ through gas of relatively low density ($n < 10^2 \text{ cm}^{-3}$), which does not contribute substantially to the observed X-ray emission. On the other hand, the velocities seen in the X-ray emission-line profiles represent the actual kinematic velocities of the shocked gas surrounding the dense clumps, which are much less than the velocity of the blast wave.

There is much more that can be done with this data set—in particular looking at the full 2D distribution of the dispersed events instead of just their 1D projection. Especially in the “stretched” MEG-minus order, one may be able to measure spatially resolved line ratios. Given the complexity of the SN 1987A system, such spatial analysis may identify emission from other geometric components of the system.

Support for this work was provided by the National Aeronautics and Space Administration through the Smithsonian Astrophysical Observatory contract SV3-73016 to MIT for support of the *Chandra* X-Ray Center, which is operated by the Smithsonian Astrophysical Observatory for and on behalf of the National Aeronautics Space Administration under contract NAS8-03060, and by *Chandra* grant GO7-8062X to the University of Colorado.

Facilities: CXO(HETG)

REFERENCES

- Aschenbach, B. 2007, in AIP Conf. Proc. 937, *Supernova 1987A: 20 Years After*, ed. S. Immler, K. W. Weiler, & R. McCray (New York: AIP), 33
- Dwek, E., & Arendt, R. G. 2007, in AIP Conf. Proc. 937, *Supernova 1987A: 20 Years After*, ed. S. Immler, K. W. Weiler, & R. McCray (New York: AIP), 58
- Haberl, F., Geppert, U., Aschenbach, B., & Hasinger, G. 2006, *A&A*, 460, 811
- Heng, K., Haberl, F., Aschenbach, B., & Hasinger, G. 2008, *ApJ*, in press
- Houck, J. C. 2002, in *High-Resolution X-Ray Spectroscopy with XMM-Newton and Chandra*, ed. G. Branduardi-Raymont (London: MSSL)
- Huenemoerder, D. P., Testa, P., & Buzasi, D. L. 2006, *ApJ*, 650, 1119
- McCray, R. 2007, in AIP Conf. Proc. 937, *Supernova 1987A: 20 Years After*, ed. S. Immler, K. W. Weiler, & R. McCray (New York: AIP), 3
- Michael, E., et al. 2002, *ApJ*, 574, 166
- Park, S., Burrows, D. N., Garmire, G. P., McCray, R., Racusin, J. L., & Zhekov, S. A. 2007, in AIP Conf. Proc. 937, *Supernova 1987A: 20 Years After*, ed. S. Immler, K. W. Weiler, & R. McCray (New York: AIP), 43
- Park, S., Zhekov, S. A., Burrows, D. N., Garmire, G. P., Racusin, J. L., & McCray, R. 2006, *ApJ*, 646, 1001
- Zhekov, S. A., McCray, R., Borkowski, K. J., Burrows, D. N., & Park, S. 2005, *ApJ*, 628, L127 (Z05)
- . 2006, *ApJ*, 645, 293 (Z06)